Inorganic Chemistry

Article

pubs.acs.org/IC

Temperature- and Pressure-Induced Phase Transitions in the Metal Formate Framework of $[ND_4][Zn(DCOO)_3]$ and $[NH_4][Zn(HCOO)_3]$

Mirosław Mączka,*[,†] Paweł Kadłubański,[†] Paulo Tarso Cavalcante Freire,[‡] Bogusław Macalik,[†] Waldeci Paraguassu,[§] Krysztof Hermanowicz,[†] and Jerzy Hanuza[†]

[†]Institute of Low Temperature and Structure Research, Polish Academy of Sciences, Box 1410, 50-950 Wrocław 2, Poland

[‡]Departamento de Física, Universidade Federal do Ceará, P.O. Box 6030, 60455-970, Fortaleza, CE, Brazil

[§]Faculdade de Física, Universidade Federal do Pará, 66075-110, Belém, PA, Brazil

Supporting Information

ABSTRACT: Vibrational properties and the temperature-induced phase transition mechanism have been studied in $[NH_4][Zn(HCOO)_3]$ and $[ND_4][Zn(DCOO)_3]$ metal organic frameworks by variable-temperature dielectric, IR, and Raman measurements. DFT calculations allowed proposing the detailed assignment of vibrational modes to respective motions of atoms in the unit cell. Temperature-dependent studies reveal a very weak isotopic effect on the phase transition temperature and confirm that ordering of ammonium cations plays a major role in the mechanism of the phase transition. We also present high-pressure Raman scattering studies on $[ND_4][Zn(DCOO)_3]$. The results indicate the rigidity of the formate ions and strong compressibility of the ZnO_6 octahedra. They also reveal the onset of a pressure-induced phase transition at about 1.1 GPa. This transition has strong first-order character, and it is associated with a large distortion of the metal formate framework. Our data indicate the presence of at least two nonequivalent formate ions in the high-pressure structure with very different C−D bonds. The decompression experiment shows that the transition is reversible.

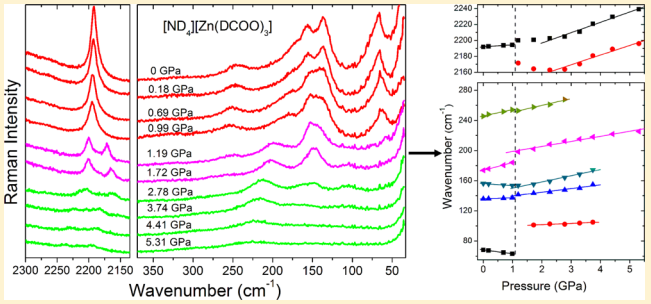

INTRODUCTION

Searching for new materials possessing both electric and magnetic orders in the same phase has become a hot topic in recent years since such materials can perform more than one task or can be manipulated by several independent stimuli.[1] Most common multiferroics are oxides.[1] However, in recent years a new emerging route for preparation of multiferroic materials was proposed, i.e., synthesis of metal−organic frameworks (MOFs) containing magnetic ions.[2] Especially attractive are MOFs with frameworks built up of MO_6 octahedra connected by the formate groups since the small size of these groups allows synthesizing compounds with relatively short distances between the magnetic ions, and thus exhibiting magnetic order at low temperatures.[2−7] MOFs have also attracted much interest due to its enormous potential for applications in gas storage, catalysis, drug delivery, sensors, electronic devices, light emitting devices, and as an anode in Li-based batteries.[8]

Among metal formate frameworks templated by mono-ammonium cations, most frequently realized frameworks have a perovskite architecture of $4^{12}\cdot6^3$ topology, in which the metal−metal connections are via *anti*−*anti* formate.[2−7] Within this class of compounds, electric order was reported for dimethylammonium metal formates of formula $[(CH_3)_2NH_2][M(HCOO)_3]$ with M = Mg, Zn, Mn, Ni, Co, Fe.[6,9−12] It has also been theoretically predicted for guanidinium compounds and $[CH_3CH_2NH_3][Mn[HCOO)_3]$.[13−15] Recently, ferroelectric properties were also reported for $[NH_4][M(HCOO)_3]$ formates, possessing a chiral framework of $4^9\cdot6^6$ topology.[16,17] It has been shown that they exhibit electric order at 191−255 K, associated with a decrease of symmetry from $P6_322$ to $P6_3$.[16,17] The observation of the good dielectric hysteresis loop below T_c confirmed that the low temperature structure of these materials is ferroelectric.[16]

It has also been reported that $[NH_4][Zn(HCOO)_3]$ exhibits negative linear compressibility and a pressure-induced phase transition.[18] The high-pressure phase at 1.35 GPa was found to be monoclinic, but details of the structure could not be solved.[18]

Although metal formate frameworks templated by mono-ammonium cations have been extensively studied using X-ray diffraction, dielectric, differential scanning calorimetry (DSC), and magnetic measurements, only a few vibrational studies have been reported. Assignment of some internal modes observed at room temperature was proposed for $[(CH_3)_2NH_2][Mn(HCOO)_3]$ by Wang et al. and later by Sanchez-Andujar et al.[3,11] Sanchez-Andujar et al. also showed a Raman spectrum of

Received: May 8, 2014
Published: August 22, 2014

   dx.doi.org/10.1021/ic501074x | *Inorg. Chem.* 2014, 53, 9615−9624

$[(CH_3)_2NH_2][Mn(HCOO)_3]$ measured at 75 K.[11] However, detailed temperature analysis of the vibrational spectra was not offered. Recently, we have applied Raman and IR spectroscopic methods to the study of order−disorder phase transitions in $[(CH_3)_2NH_2][M(HCOO)_3]$ with M = Zn, Fe, Ni, Mn and a more detailed assignment was proposed, including lattice modes and IR active modes.[19] In the family of $[NH_4][M(HCOO)_3]$ compounds, partial assignment was proposed for Mn, Co, and Ni compounds only for IR active internal modes.[16] A more detailed assignment and temperature dependence of IR and Raman bands have recently been reported by us for $[NH_4][Mg(HCOO)_3]$.[17]

Studies of $[NH_4][M(HCOO)_3]$ crystals showed the importance of the rotational dynamics of the NH_4^+ ions in the temperature-induced phase transition mechanism.[16,17] However, a detailed mechanism of the phase transition is still not fully understood. In order to interpret a phase transition mechanism in crystals possessing extensive H-bonds, it is important to study the influence of isotopic substitution on phase transition temperature. It is also worth adding that isotopic substitution greatly facilitates assignment of modes to the respective motions of atoms in the unit cell. Furthermore, vibrational spectroscopy may provide deeper insight into both temperature- and pressure-induced phase transition mechanisms since it is particularly suited to studies of H-bonds, order−disorder, and displacive phase transitions.[20−22]

In this work, we report the synthesis of $[NH_4][Zn(HCOO)_3]$ and not previously reported $[ND_4][Zn(DCOO)_3]$ and their dielectric properties. We also report a differential scanning calorimetric (DSC) study of the deuterated sample and DFT calculations for both compounds in order to better understand the vibrational properties of this class of compounds. Having discussed the assignments of modes, we then report temperature-dependent Raman scattering and infrared (IR) studies of $[NH_4][Zn(HCOO)_3]$ and $[ND_4][Zn(DCOO)_3]$ in order to obtain information on the microscopic mechanism of the temperature-induced structural phase transition occurring in these compounds. In the last part of the work, we report a high-pressure Raman scattering study of $[ND_4][Zn(DCOO)_3]$ to probe pressure-induced structural changes in this material. We would like to emphasize that Raman studies under pressure have not yet been reported for any member of the metal formates templated by an organic cation. The highest pressure reached in our experiment for $[ND_4][Zn(DCOO)_3]$, 5.31 GPa, is significantly higher than the 1.35 GPa pressure reached in the reported X-ray diffraction experiment on $[NH_4][Zn(HCOO)_3]$.[18]

EXPERIMENTAL SECTION

Synthesis. $ZnCl_2$ (98%, Fluka), ammonium-d_4 deuteroxide solution (25 wt %, 99 atom % D, methanol-d_4 (99.96 atom % D, Aldrich), formic acid-d_2 (95 wt % in D_2O, Aldrich), $[NH_4][HCOO]$ (99%, Fluka), methanol (99.8%, Aldrich), and formic acid (98%, Fluka) were commercially available and used without further purification. $[ND_4][Zn(DCOO)_3]$ was obtained by a slow diffusion method. First, 12.8 mmol of formic acid-d_2 was added dropwise to 20 mmol of ammonium-d_4 deuteroxide solution. The mixture was dried at 70 °C, and the obtained white powder of $[ND_4][DCOO_3]$ was dissolved in16 mL of methanol-d_4 solution containing 7 mmol of formic acid-d_2. This solution was placed at the bottom of a glass tube (9 mm inner diameter). Into this solution, 16 mL of methanol-d_4 solution containing 1.6 mmol of $ZnCl_2$ were gently added. The tube was sealed and kept undisturbed. Colorless crystals were harvested after 5 days. The yield is about 65% based on the starting zinc salt. The product was washed by methanol-d_4 and dried at 60 °C. Synthesis of $[NH_4][Zn(HCOO)_3]$ was performed in a similar way with the difference that the solution placed at the bottom of a glass tube contained 16 mL of methanol, 12.8 mmol of $[NH_4][HCOO]$, and 12.8 mmol of formic acid. Colorless crystals were harvested after 10 days. The yield is about 70% based on the starting zinc salt. The product was washed by methanol and dried at 60 °C.

Powder X-ray Diffraction. XRD pattern was obtained on an X'Pert PRO X-ray diffraction system equipped with a PIXcel ultrafast line detector, focusing mirror, and Soller slits for Cu$K\alpha_1$ radiation (λ = 1.54056 Å).

DSC. The DSC measurements of $[ND_4][Zn(DCOO)_3]$ were performed on a DSC-7 instrument (PerkinElmer) under a nitrogen atmosphere with two cycles using 7.33 mg of a powdered sample. The temperature range was 100−350 K, and the cooling and heating rates were 15 °C/min.

Dielectric Properties. The complex dielectric permittivity was measured at a frequency range from 10^0 to 10^6 Hz using a broad-band impedance Alpha analyzer with an Active Sample Cell (Novocontrol). The measurements were performed every 1 K in the 110−373 K range on pellets made of well-dried samples. The pellets had a diameter of 6 mm and a thickness of 0.6 mm, and they were placed between gold electrodes with diameter of 6 mm. The temperature was changed by the flow of vaporized liquid nitrogen heated and controlled by a self-made heating system. The temperature stability was about ±0.2 K.

Raman and IR Studies. Temperature-dependent Raman spectra were measured using a Bruker FT 100/S spectrometer with YAG:Nd laser excitation (1064 nm) and a helium-flow Oxford cryostat. Temperature dependent IR spectra were measured on a Biorad 575C spectrometer using a helium-flow Oxford cryostat. In the 3800−400 cm^{-1} range, a Fluoroluble (Nujol) suspension was used for $[NH_4][Zn(HCOO)_3]$ ($[ND_4][Zn(DCOO)_3]$) whereas for the 500−50 cm^{-1} range the samples were in an Apiezon N suspension. The spectral resolution was 2 cm^{-1}.

The high pressure Raman spectra were recorded using a microscope attached to a triple-grating spectrometer Jobin Yvon T64000 on an about 10 μm thick platelet of the $[ND_4][Zn(DCOO)_3]$ single crystal through backscattering geometry. The 514.5 nm line of an argon laser was used as excitation, and the spectrometer slits were set for a resolution of 2 cm^{-1}. No analyzer was used in the high-pressure experiment. In order to reach high pressures, the samples were loaded into a diamond anvil cell from EasyLab with diamond of 0.35 mm of culets. A stainless steel gasket with a thickness of 200 μm was preindented to 50 μm, and a 100 μm hole was drilled in the center of the indentation by using an electric discharge machine from EasyLab. The Nujol served as the pressure transmitting media. Pressures were measured based on the shifts of the ruby R1 and R2 fluorescence lines.

Computational Methods. Theoretical studies have been performed for two models of the investigated systems at zero K: the NH_4^+ (ND_4^+) cation in the dimeric complex unit (model 1) and the monomeric $[Zn(HCOO)_6]^{4-}$ ($[Zn(DCOO)_6]^{4-}$) unit (model 2) (see Figures S1 and S2, Supporting Information). The three-parameter hybrid B3LYP density functional method has been used with the 6-31G(d,p) basis set for all atoms of the ligands.[23] The 6-31G(d,p) basis set was chosen since it allows performing good quality calculations of vibrational properties in a reasonable time. In particular, this basis set was very often used for the calculations of vibrational spectra of many anionic species, including formates.[24] Furthermore, DFT calculations of vibrational properties for an isolated formate ion using five different levels of basis sets showed that although using the larger basis sets improved the results, the rms error decreased less than 3% when the 6-311++G(2d,p) basis set was used instead of the 6-31G(d,p) one.[25] Some other papers also showed that the increased size of the basis set did not affect the assignment of modes due to weak changes in the calculated wavenumbers.[26] Thus, the choice of the 6-31G(d,p) basis set is a good compromise between the quality of DFT calculations and computational time.

For the Zn atom the LanL2DZ effective core potential with the concomitant valence basis set was applied.[27] The Zn(II) complexes are the closed-shell systems. Therefore, all calculations were based on a

dx.doi.org/10.1021/ic501074x | Inorg. Chem. 2014, 53, 9615−9624

restricted mechanism; however, for clarity, R will be omitted from the RB3LYP abbreviation, in the remaining text. For the monomeric species, $[Zn(HCOO)_6]^{4-}$ and $[Zn(DCOO)_6]^{4-}$, full geometry optimizations were followed by the calculations of vibrational frequencies as well as infrared and Raman scattering activities (S_R). The theoretical Raman intensities (I_R) were obtained from the calculated S_R values using the laser excitation frequency 9398.5 cm^{-1} (1064 nm, Nd: YAG laser).[28] For $[NH_4][Zn(HCOO)_6]_2^{7-}$ and $[ND_4][Zn(DCOO)_6]_2^{7-}$, a partial geometry optimization has been performed. The geometry of the NH_4^+ and ND_4^+ cations was fully optimized, in the frame of the two connected zinc complexes whereas the geometrical parameters of two bonded Zn(II) complexes were taken from literature data.[16] The calculated frequencies of the NH_4^+ and ND_4^+ cations in this model were real, which confirmed the stable structure. All computations were carried out with the Gaussian 09 set of programs.[29] It is worth adding that we have not taken into account in our DFT calculations the dispersion interactions. It is well-known that incomplete treatment of dispersive interactions may significantly affect the accuracy of DFT calculations for those systems, for which dispersive interactions are significant, for instance, in biological systems and weakly bound molecular complexes.[30] Since using dispersion correction influences the calculated structural parameters, it also affects the calculated vibrational frequencies. For instance, DFT studies of TiO_2 anatase and ammonium perchlorate showed that, in comparison with standard DFT, the disperison correction led to shifts of nearly all frequencies toward higher values.[31] However, the ν_1, ν_2, and ν_4 modes of NH_4^+ ions showed an opposite behavior. Although the dispersion correction improved the agreement between the theoretical and experimental data for ammonium perchlorate, the improvement was small and all modes were calculated within 5% of experiment irrespective of the choice of pseudopotentials or the dispersion correction scheme.[31] Since as in the case of ammonium perchlorate the compounds studied here are also ionic materials, a dispersion correction is expected to have a weak effect on the calculated vibrational frequencies.

RESULTS AND DISCUSSION

Powder X-ray Diffraction and Thermal Properties. The experimental powder XRD patterns measured for the $[NH_4][Zn(HCOO)_3]$ and $[ND_4][Zn(DCOO)_3]$ crystals are in very good agreement with the calculated ones based on the single-crystal structure of $[NH_4][Zn(HCOO)_3]$ reported by Xu et al. (Figure S3, Supporting Information).[16] This result confirms the phase purity of the bulk samples.

The DSC measurements of $[ND_4][Zn(DCOO)_3]$ show an anomaly at approximately 191 K upon heating and 190 K upon cooling (Figure S4). The shape of this anomaly is very similar to that observed for other $[NH_4][M(HCOO)_3]$ formates with M = Mn, Co, Fe, Ni, Zn, and Mg,[16,17] suggesting a second-order, reversible phase transition. The associated changes in enthalpy ΔH and entropy ΔS are ~0.67 kJ mol^{-1} and ~3.51 J mol^{-1} K^{-1}, respectively. These values are slightly larger than the ~0.2−0.5 kJ mol^{-1} (<2 J mol^{-1} K^{-1}) values reported for other $[NH_4][M(HCOO)_3]$ compounds.[16,17] It is important to mention that for $[NH_4][Zn(HCOO)_3]$ the phase transition was reported to be 192 K in the heating mode.[16] As can be noticed, the isotope effect for this compound is very small. A very weak isotope effect was previously reported also for dimethylammonium analogues, that is, $[(CH_3)_2NH_2][Co(HCOO)_3]$ and its perdeutero analogue $[(CD_3)_2ND_2][Co(DCOO)_3]$, and $[(CH_3)_2ND_2][M(HCOO)_3]$ with M = Mn, Ni.[9,19] Thus, the new important information derived from the DSC studies of the deuterated sample is that, as in the case of the family of dimethylammonium metal formates, also in the family of ammonium metal formates the movement of the proton (deuteron) along the N−H···O (N−D···O) bonds can be excluded as the microscopic origin of the phase transition.

Dielectric Properties. Figure 1 shows the temperature dependence of the real component ε' of the dielectric constant

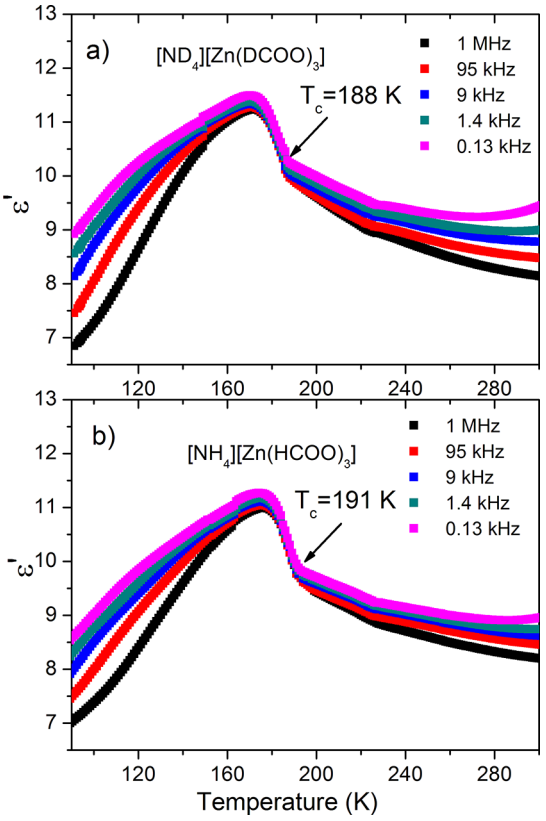

Figure 1. Temperature-dependent traces of the real part of the dielectric permittivity, ε', for powdered (a) $[ND_4][Zn(DCOO)_3]$ and (b) $[NH_4][Zn(HCOO)_3]$ at 0.13, 1.4, 9, 95, and 1000 kHz.

of powdered $[ND_4][Zn(DCOO)_3]$ and $[NH_4][Zn(HCOO)_3]$. Broad dielectric anomalies, corresponding to the phase transitions, are clearly seen for both compounds. Former studies of $[NH_4][Zn(HCOO)_3]$ showed the presence of a strong and narrow dielectric anomaly at 191 K under applied electric field E||c for a single crystal but a much weaker and broader anomaly with the maximum shifted toward lower temperatures for the powdered sample.[10] This anomaly was attributed to the onset of a ferroelectric order in the low temperature phase, and the ferroelectricity of $[NH_4][Zn(HCOO)_3]$ was confirmed by the presence of a very clear dielectric hysteresis loop.[10,16] Our broad anomalies are very similar to that reported previously for powdered $[NH_4][Zn(HCOO)_3]$. Figure 1 shows that the dielectric anomaly for $[ND_4][Zn(DCOO)_3]$ shifts by only 3 K toward lower temperature in comparison with $[NH_4][Zn(HCOO)_3]$. Former dielectric data on $[NH_4][Zn(HCOO)_3]$ have not provided information on the relaxation phenomena in this crystal. Our data show that the dielectric loss tan δ shifts to higher temperatures with increasing temperatures (Figure S5). This shift in peak position of tan δ can be attributed to rotational motions of NH_4^+ (ND_4^+) cation in the cavities of the framework. The frequency dependent tan δ was examined for an Arrhenius type behavior, $\tau = \tau_0 \times \exp(E_a/k_BT)$, where E_a is the activation energy barrier between two thermodynamically equivalent sites for NH_4^+ (ND_4^+) reorientational motion. Insets

dx.doi.org/10.1021/ic501074x | Inorg. Chem. 2014, 53, 9615−9624

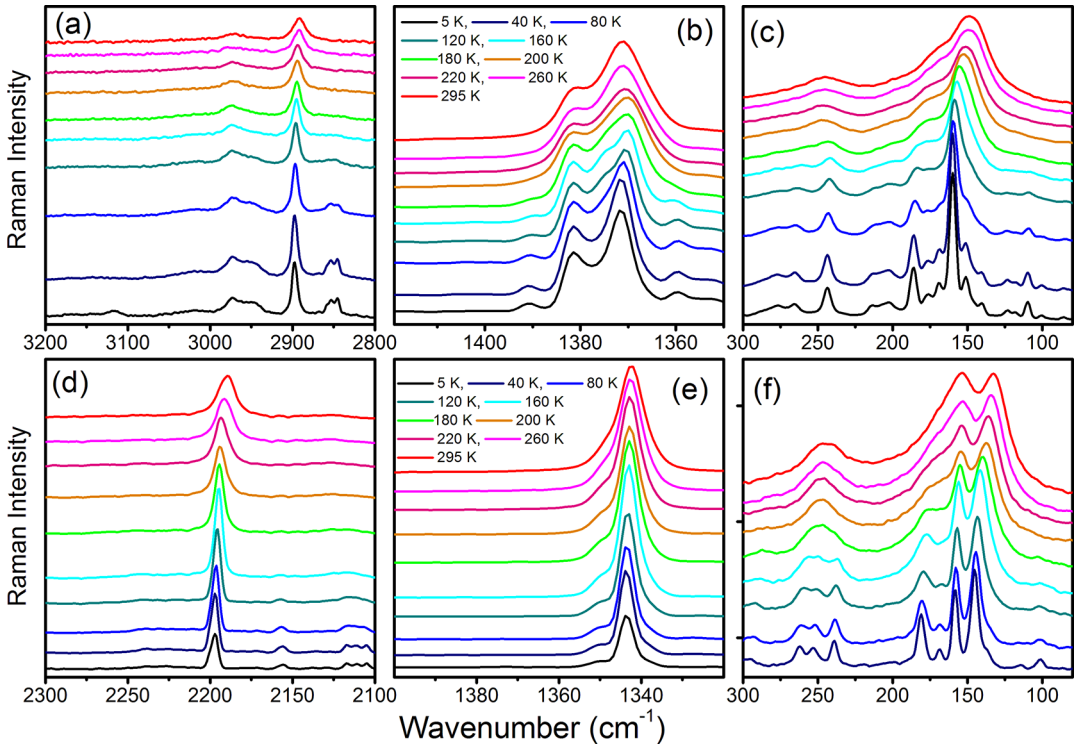

Figure 2. Detail of the Raman spectra results corresponding to the spectral ranges 2800−3200, 1350−1420, and 80−300 cm^{-1} for $[NH_4][Zn(HCOO)_3]$ (a, b, and c) and spectral ranges 2100−2300, 1320−1400, and 80−300 cm^{-1} for $[ND_4][Zn(DCOO)_3]$ (d, e, and f).

in Figures S5 show that the dielectric relaxation observed below T_c obeys the Arrhenius law, with $\tau_0 = 1.58 \times 10^{-14}$ s and $E_a/k_B = 1.83 \times 10^3$ K ≈ 0.16 eV for $[ND_4][Zn(DCOO)_3]$ and $\tau_0 = 1.21 \times 10^{-14}$ s and $E_a/k_B = 1.92 \times 10^3$ K ≈ 0.17 eV for $[NH_4][Zn(HCOO)_3]$. The obtained values of the activation energies are significantly smaller than the 0.28 eV value reported for $[NH_4][Mg(HCOO)_3]$.[17] This result indicates significantly weaker bonding of the ammonium cations to the zinc formate framework compared to the magnesium formate framework.

Vibrational Studies - Selection Rules, DFT Calculations and Assignment of Modes. The vibrational spectra of $[NH_4][Zn(HCOO)_3]$ and $[ND_4][Zn(DCOO)_3]$ can be regarded as composed of internal vibrations of the ammonium and formate ions, and the lattice vibrations. Table S1, Supporting Information, shows the correlation between the optical modes in the $P6_322$ and $P6_3$ structures. Since the NH_4^+ (ND_4^+) cations are disordered in the $P6_322$ phase, we do not present distribution of the internal modes of these ions among the irreducible representations for this structure. The calculated wavenubers for the above-described models as well as experimental wavenumbers for $[NH_4][Zn(HCOO)_3]$ and $[ND_4][Zn(DCOO)_3]$ are presented in Tables S2 and S3, Supporting Information.

Let us now discuss the assignments of modes. The N−H and N−D stretching vibrations (ν_1 and ν_3) of free molecules were reported to appear in the region 3300−3500 and 2400−2600 cm^{-1}, respectively (the frequency isotopic ratio ν(N−H)/ν(N−D) is close to 1.41).[32] The formation of H-bonds should result in significant changes, that is, a shift of the stretching modes to lower frequencies, an increase in the intensity and width of the corresponding vibrational bands, and a decrease of the isotopic ratio.[20] The bending modes ν_2 and ν_4 of the ammonium cation were located near 1600−1720 and 1390−1460 cm^{-1} (1100−1300 and 1050−1150 cm^{-1}) for NH_4^+ (ND_4^+), respectively.[33] Our experimental room temperature data show the N−H (N−D) stretching modes in the region 2847−3337 cm^{-1} (2154−2483 cm^{-1}) (see Table S3); i.e., some of these bands have wavenumbers close to the free ammonium cations, but others are shifted toward lower frequencies even by 400−500 cm^{-1} (in respect to the stretching frequencies of N−H and N−D bonds not involved in the formation of H-bonds). The wavenumber isotopic ratio is about 1.32−1.34. The observed shifts and value of the isotopic ratio indicate that the ammonium cations form medium strength H-bonds with the anionic framework. Tables S2 and S3 show that the calculated frequencies of the ammonium cation are in quite good agreement with the experimental values. It is worth noting that although assignment of the stretching modes is straightforward, assignment of the bending modes of the ND_4^+ cations is more difficult since the frequency ranges where these modes are observed may overlap. Our DFT calculations show, however, that in the present case the energy gap between the the ν_2 and ν_4 modes should be about 50 cm^{-1} (see Table S2). Moreover, DFT calculations predict that the intensity of the IR bands corresponding to the ν_2 modes should be significantly smaller than the intensity of the ν_4 bands (Table S2). Thus, DFT calculations allow us to propose a more precise assignment of the bending modes of the deuerated ammonium cation.

Regarding the internal modes of the $HCOO^-$ ions, our DFT calculations show that these modes should appear near 2811−2826 cm^{-1} (ν_1), 1685−1735 cm^{-1} (ν_4), 1405−1413 cm^{-1} (ν_5), 1363−1369 cm^{-1} (ν_2), 1064−1074 cm^{-1} (ν_6), and 764−768 cm^{-1} (ν_3). The ν_1, ν_5, ν_2, ν_6, and ν_3 calculated modes are in very good agreement with the experimental spectra that show the bands near 2887−2891, 1380−1382, 1368−1371, 1075, and 803−809 cm^{-1}, respectively. The calculated values for the

dx.doi.org/10.1021/ic501074x | Inorg. Chem. 2014, 53, 9615−9624

ν_4 mode are, however, overestimated since the corresponding bands are observed near 1567−1576 cm^{-1}. Deuteration is expected to have a strong impact on the ν_1, ν_5, and ν_6 modes of the $HCOO^-$ ions since these modes correspond to the C−H stretching, C−H in-plane bending mode, and C−H out-of-plane bending modes, respectively.[25,34] Assignment of the ν_1 modes of the $DCOO^-$ ion is straightforward, but DFT calculations are very useful in assigning the ν_5 and ν_6 modes. As can be noticed, the experimental (theoretical) data are consistent with the expected downshift of modes after deuteration; that is, the ν_1, ν_5, and ν_6 modes are observed (calculated) at 2189, 1021−1024, and 913−914 cm^{-1} (2065−2078, 1034−1036, and 916−922 cm^{-1}). It is worth mentioning that deuteration also leads to a downshift of the ν_2 mode by nearly 30 cm^{-1} and the ν_3 mode by 8 cm^{-1} (see Table S3). This result indicates that although they correspond to vibrations of the C−O bonds, the C−H vibrations contribute weakly to these modes.

An assignment of lattice modes was proposed previously for many formates and compounds containing ammonium cations.[33,35] Thus, translational and librational modes of NH_4^+ (ND_4^+) cations were located in the 160−270 and 300−480 cm^{-1} (140−250 and 310−380 cm^{-1}) region, respectively.[33,35] Translations and librations of the formate ions were usually observed below 250 cm^{-1}.[36] As can be noticed, some modes may appear in broad frequency ranges. Moreover, vibrational modes my couple to each other and precise assignment of lattice modes through comparison of vibrational spectra of different compounds is difficult. Our DFT calculations allow us to propose a more detailed assignment of the lattice modes. For instance, they show that the most intense IR bands correspond mainly to translations of the Zn^{2+} cations. They also allow distinguishment between librational and translational modes of the formate units and show that the most intense Raman bands can be attributed mainly to librational motions of the formate units (see Table S3). It is also worth noting that our DFT calculations predict well that the librational modes of the ammonium ions should be observed at higher frequencies than the translational modes.

Temperature-Dependent Raman and IR Studies, and Mechanism of the Temperature-Induced Phase Transition. Temperature-dependent Raman and IR spectra are presented in Figures 2 and S6−S11. In order to better observe the temperature dependent changes in vibrational spectra, we also present plots of frequencies and full width at the half-maximum (fwhm) values for a number of structural units (Figures 3, 4, and S12−S14).

Figure S12 shows weak anomalies near T_c for $[NH_4][Zn(HCOO)_3]$, that is, a change in the slope of wavenumbers vs temperature for the ν_1 and ν_5 modes of the $HCOO^-$ ion, and splitting for the ν_2 and ν_6 modes. Clear splitting is also observed for the coupled $T'(HCOO^-)$ and $T'(Zn^{2+})$ mode (see Figure S14a). This behavior points to distortion of the metal formate framework due to the ferroelectric phase transition. It is worth noting that according to the X-ray diffraction data there is only one unique $HCOO^-$ ion in the high-temperatrure phase but three distinct ions in the low temperature phase.[14] Thus, the observed splitting reflects the appearance of nonequivalent $HCOO^-$ ions. Interestingly, we observe very clear splitting for the ν_6 mode, which corresponds to the C−H out-of-plane bending mode. This behavior suggests the presence of different C−H bonds in the low-temperature phase although the reported X-ray diffraction data showed the same C−H bond lengths for all three crystallographically nonequivalent $HCOO^-$ ions.[16] This discrepancy between the Raman and X-ray diffraction data is due to the inaccuracy of X-ray diffraction on the position of hydrogen atoms, and it shows that vibrational spectroscopy is a very valuable method for studies of C−H bonds. It is worth noting that the observed splitting is about two times smaller than that reported for $[NH_4][Mg(HCOO)_3]$.[17] This behavior indicates that the distortion of the metal formate framework due to the ferroelectric transition is much smaller for $[NH_4][Zn(HCOO)_3]$ when compared to $[NH_4][Mg(HCOO)_3]$.

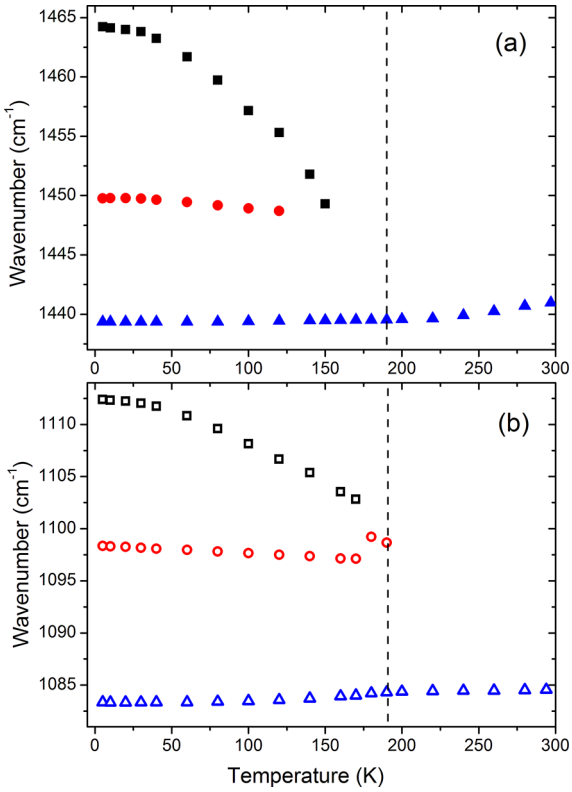

Figure 3. Temperature dependence of the ν_4 mode of NH_4^+ for (a) $[NH_4][Zn(HCOO)_3]$ and (b) $[ND_4][Zn(DCOO)_3]$. The vertical lines indicate the temperature at which $[NH_4][Zn(HCOO)_3]$ or $[ND_4][Zn(DCOO)_3]$ undergoes the phase transition.

Figures S13 and S14 show that clear anomalies near T_c are also observed for $[ND_4][Zn(DCOO)_3]$. However, we cannot observe any clear splitting for the ν_2 mode and splitting of the translational mode near 245 cm^{-1} is significantly smaller when compared to $[NH_4][Zn(HCOO)_3]$. This result suggests that the deuterated sample exhibits a smaller distortion of the framework during the phase transition.

Let us now discuss the temperature dependence of the ammonium cation vibrational modes. Figure S6 shows that upon cooling the narrow (broad) IR bands above 3300 cm^{-1} (in the 2800−3200 cm^{-1} range) shift to higher and lower wavenumbers, respectively. This behavior is accompanied by significant changes in intensities, narrowing and splitting of the NH_4^+ bands (see Figures 2, 3, S10, and S11). The temperature dependence of the NH_4^+ modes of $[NH_4][Zn(HCOO)_3]$ is very similar to that observed for the Mg analogue and can be attributed to the increased strength of the H-bonds.[17] However, the observed shifts upon cooling are more pronounced for the Zn compound, suggesting more significant changes in strength of the H-bonds upon cooling in this compound. Raman and IR

dx.doi.org/10.1021/ic501074x | Inorg. Chem. 2014, 53, 9615−9624

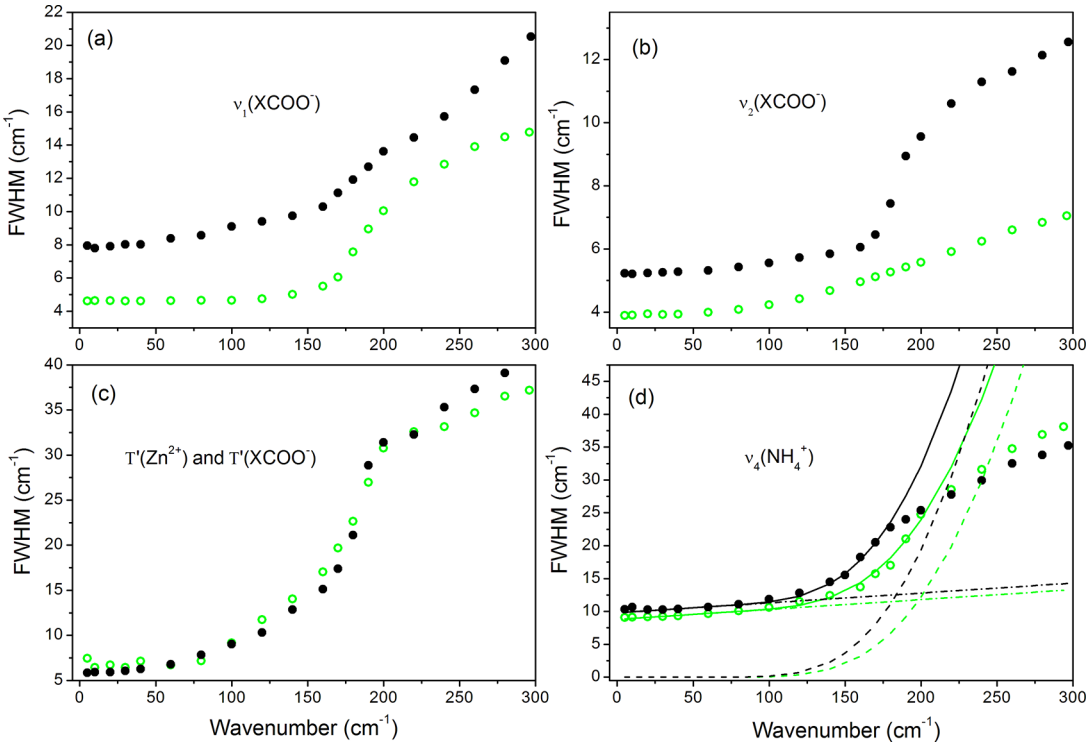

Figure 4. Temperature dependence of fwhm of (a) the 2891 cm^{-1} (full circles) and 2189 cm^{-1} (open circles) Raman bands corresponding to the $\nu_1(XCOO^-)$ mode, (b) 1371 cm^{-1} (full circles) and 1342 cm^{-1} (open circles) Raman bands corresponding to the $\nu_2(XCOO^-)$ mode, (c) the 244 (full circles) and 245 cm^{-1} (open circles) Raman bands corresponding to the coupled T′($XCOO^-$) and T′(Zn^{2+}) modes, and (d) the 1440 (closed circles) and 1084 cm^{-1} (open circles) IR bands corresponding to the $\nu_4(NX_4^+)$ mode. The solid lines in (d) are fits of the data to eq 1. The dash dot and dash lines represent contribution due to anharmonicity and reorientational processes, respectively.

bands of $[ND_4][Zn(DCOO)_3]$ also exhibit significant shifts, narrowing, and splitting that can be attributed to a change in the H-bond strength upon cooling (see Figures 2, 3, S7, and S11).

In order to obtain further information on the mechanism of the phase transition, we proceed now to the discussion of the temperature dependence of fwhm values for selected modes. Figure 4 shows that the ν_1 and ν_2 bands of the formate ion are significantly narrower for the deuterated sample. This behavior can be attributed to the reduced mean amplitude of the vibration of D atoms when compared to H atoms. The fwhm of these modes exhibits a significant increase above 150 K, i.e., about 40 K below T_c. An even more pronounced increase in fwhm upon heating occurs for the lattice bands near 245 cm^{-1} and the $\nu_4(NX_4^+)$ bands (see Figure 4). As discussed previously, such a pronounced increase in fwhm indicates that the phase transition in the studied compounds has an order−disorder character and is associated with the rotational dynamics of the ammonium cations.[17] In such a case, the temperature dependence of fwhm can be approximated by

$$\mathrm{FWHM} = \mathrm{A} + \mathrm{BT} + \mathrm{C}\exp(-E_a/kT) \quad (1)$$

where E_a is the activation energy, k is the Boltzmann constant, and T is the temperature.[21] The value of the first term depends on structural and compositional defects. The linear term BT represents the influence of phonon−phonon anharmonic interactions, and the last term gives information on thermally activated reorientational processes. Figure 4d shows that the temperature dependence of fwhm values of the $\nu_4(NX_4^+)$ modes can be well approximated by eq 1 with the activation energy E_a equal to 86 meV for $[NH_4][Zn(HCOO)_3]$ and 93 meV for $[ND_4][Zn(DCOO)_3]$. The reorientational processes in $[NH_4][Zn(HCOO)_3]$ and $[ND_4][Zn(DCOO)_3]$ start to contribute to the observed fwhm at a significantly lower temperature (above 100 K) than in the Mg analogue (140 K).[17] Moreover, the estimated $E_a \approx 86$ meV of $[NH_4][Zn(HCOO)_3]$ is significantly smaller than the 103 meV value found for $[NH_4][Mg(HCOO)_3]$.[17] The smaller value of E_a and the above-discussed temperature suggest weaker binding of the NH_4^+ cation in the $[NH_4][Zn(HCOO)_3]$ structure. This conclusion corroborates with a lower phase transition temperature into the disordered phase for the Zn compound (191 K), when compared to the Mg compound (255 K).[17] It is interesting to note that E_a increases upon deuteration. A similar effect was also observed for the dimethylammonium analogues.[19] It is known that if the potential curve for the motion of ND_4^+ equals that of NH_4^+, the activation energy for the reorientation is expected to increase by the deuteration due to the increase of the moment of inertia.[37] Thus, the observed increase of E_a for $[ND_4][Zn(DCOO)_3]$ is consistent with the increase of the moment of inertia for ND_4^+ ions and weak change of the potential curve for the motion of ammonium cation. This suggests that the interaction between the ammonium cations and anionic framework are weakly affected by the deuteration. Figure 4 also shows that the deuteration has a negligible effect on phonon−phonon anharmonic interactions.

High Pressure Raman Scattering Study of $[ND_4][Zn(DCOO)_3]$, and Mechanism of the Pressure-Induced Phase Transition. The pressure-dependent Raman spectra are presented in Figure S15, but the overall changes in the Raman spectra can be better followed by analyzing the

dx.doi.org/10.1021/ic501074x | Inorg. Chem. 2014, 53, 9615−9624

wavenumber (ω) vs pressure (P) plot shown in Figure 5. Figure 5 shows that the pressure dependence of all vibrational

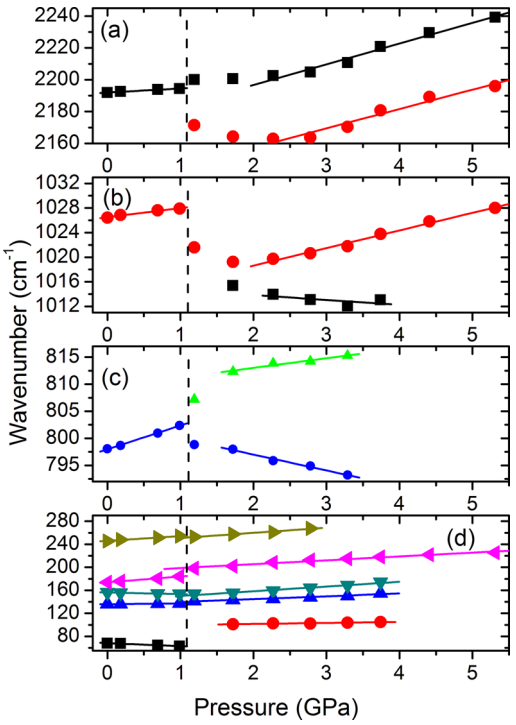

Figure 5. Wavenumber vs pressure plots of the Raman modes observed in $[ND_4][Zn(DCOO)_3]$ crystal for compression experiment. The vertical lines indicate the pressures at which $[ND_4][Zn(DCOO)_3]$ undergoes phase transitions. The solid lines are linear fits on the data to $\omega(P) = \omega_0 + \alpha P$.

modes, except for the 1.19−1.72 GPa range for the high wavenumber modes, can be well described using a linear function $\omega(P) = \omega_0 + \alpha P$. The results for pressure coefficients ($\alpha = d\omega/dP$) and wavenumber intercepts at zero pressure (ω_0), obtained from fitting of the experimental data through the least-squares method, are listed in Table 1. Table 1 also summarizes the mode Grüneisen parameters $\gamma_i = B_0/\omega_i \cdot \partial\omega_i/\partial P$, where B_0 is the bulk modulus. The mode Grüneisen parameters have been

Table 1. Raman Wavenumbers ω_0 for the Two Phases of $[ND_4][Zn(DCOO)_3]$ along with Pressure Coefficients α Obtained from the Linear Fits on the Data to $\omega(P) = \omega_0 + \alpha P$

ambient pressure phase			high-pressure phase	
ω_0 (cm^{-1})	α (cm^{-1} GPa^{-1})	γ	ω_0 (cm^{-1})	α (cm^{-1} GPa^{-1})
2191.9	2.54	0.038	2170.7	13.01
			2132.9	12.16
1026.5	1.47	0.047	1012.9	2.87
			1015.4	−0.78
798.0	4.42	0.18	802.9	−2.94
			809.4	1.79
246.0	8.25	1.1	242.0	8.96
173.8	10.26	1.94	192.0	6.71
156.2	−2.79	−0.59	142.0	8.19
135.8	1.44	0.35	134.9	4.92
68.2	−5.15	−2.48	98.2	1.71

calculated using B_0 = 32.8 GPa obtained from high-pressure X-ray diffraction studies.[18]

Figure S15 shows that, on applying pressure, the spectra remain qualitatively the same up to 0.99 GPa. Figure 5 and Table 1 show that, in this pressure range, wavenumbers of the majority of modes increase. However, the modes at 68 and 156 cm^{-1} exhibit a negative pressure dependence. Especially pronounced softening is noticed for the 68 cm^{-1} band that can be attributed to librational motions of the $HCOO^-$ ions and for which the coefficient α is −5.15 cm^{-1}/GPa. Pronounced softening of modes under pressure reveals that anharmonicity becomes important, and it is an indication of some crystal instability.[38] Inspection of Table 1 also shows that the mode Grüneisen parameters of the 2192 and 1026 cm^{-1} modes (C−D stretching and bending mode of the $DCOO^-$ ions, respectively) are very small. A larger value is found for the 798 cm^{-1} mode (O−C−O bending), but the largest values are observed for the lattice modes. The obtained Grüneisen parameters indicate, therefore, that under applied pressure the C−D and C−O bonds of the $DCOO^-$ ions shorten weakly but significant shortening occurs for the Zn−O bonds. In other words, the observed behavior indicates rigidity of the formate ion and large compressibility of ZnO_6 octahedra.

When the pressure reaches 1.19 GPa, the Raman spectrum changes drastically. The most characteristic changes are (i) discontinuous wavenumber shifts, (ii) very clear changes in the slope of wavenumbers vs pressure, (iii) splitting of the internal modes into doublets, and (iv) a change in the intensity of many bands (Figures 5 and S15). The observed modifications of the Raman spectra indicate that a first-order phase transition takes place in $[ND_4][Zn(DCOO)_3]$ near about 1.1 GPa. The observed splitting of internal modes points to the lower symmetry of the high-pressure phase. This conclusion is in agreement with the postulated monoclinic distortion of the structure on the basis of X-ray diffraction results.[18] It is important to mention that the phase transition in $[NH_4][Zn(HCOO)_3]$ occurred somewhere between 0.94 and 1.35 GPa.[18] Our results showing phase transition for the deuterated analogue near 1.1. GPa indicate, therefore, the weak effect of deuteration on the phase transition pressure. We would also like to emphasize that the structure of the high-pressure phase could not be solved due to the limited number of reflections and, therefore, structural details of the high pressure phase are not known.[18] Our Raman data give, however, new interesting information on the pressure-induced structural changes. (1) The structure of the high-pressure phase is different from that observed at ambient pressure and low temperatures. In particular, in the low-temperature structure the distortion of the metal formate framework is weak and the ammonium cations are ordered. The very large splitting of the $DCOO^-$ internal modes and large width of Raman bands indicate that the metal formate framework is very strongly distorted in the high-pressure phase whereas the ammonium cations remain disordered. Splitting of the internal modes into doublets indicates the presence of at least two nonequivalent $DCOO^-$ ions in the high-pressure phase with significantly different C−D and C−O bond lengths. (2) The splitting of the 1026 and 798 cm^{-1} increases upon further compression. This result indicates that the metal formate framework distortion becomes larger when pressure increases beyond 1.19 GPa. However, the spectra remain qualitatively similar, suggesting that no other phase transition occurs in this material up to 5.31 GPa. (3) It is interesting to note that the bands corresponding to the C−D

dx.doi.org/10.1021/ic501074x | Inorg. Chem. 2014, 53, 9615−9624

stretching and bending vibrations exhibit a shift toward lower wavenumbers at the phase transition. Such behavior indicates that the C−D bond lengths increase in the high-pressure phase. The origin of this behavior is not clear, but it points to significant rearrangements of the formate units in the high-pressure phase. (4) Our data show that upon an increase of pressure beyond 1.19 GPa, the bands become broader and very few broad bands can be observed at 5.31 GPa. Such behavior suggests that pressure induces amorphization of the studied sample. (5) As we have already mentioned, wavenumbers of the internal modes exhibit departure from the linear dependence of wavenumbers vs pressure at 1.19 and 1.72 GPa. Interestingly, the 2170 and 1022 cm^{-1} components (at 1.19 GPa) exhibit softening when the pressure increases to 1.72 GPa and hardening above 2 GPa (see Figure 5). This behavior might indicate the presence of another subtle structural phase transition near 2 GPa, but confirmation of this transition would require additional studies using other experimental methods. (6) It is worth noting that the pressure coefficients α are still large for many modes of the high-pressure phase. This result indicates that the high-pressure phase is still strongly compressible. However, this high pressure phase which is stable above 1.1 GPa does not show any negative pressure dependence of the lattice modes, confirming the high stability of this structure.

In order to gain more insight into the mechanism of the phase transition, we have also performed Raman studies of the $[ND_4][Zn(DCOO)_3]$ crystal during the decompression. Figure S15a shows that, upon releasing pressure, splitting of the $\nu_1(DCOO^-)$ and $\nu_5(DCOO^-)$ bands near 1200 and 1030 cm^{-1} disappears and the bands after decompression are observed at the same frequencies as the corresponding bands of the initial phase before compression. The lattice bands also return to their initial frequencies (see Figures S15c and S16), thus indicating the reversibility of the process. However, the spectrum is less intense, Raman bands are broader, and there are some changes in relative intensities of the Raman bands. Such behavior is often observed in the high pressure studies of single crystals strongly undergoing first-order phase transitions due to reorientation of a sample during the decompression experiment and creation of domains and/or defects.[38,39]

Let us now discuss the mechanism of the pressure-induced phase transition. Our results show that application of pressure leads to tilts of the rigid $DCOO^-$ ions and significant shortening of Zn−O distances. This behavior is consistent with the X-ray diffraction studies performed for $[NH_4][Zn(HCOO)_3]$; that is, these studies revealed no significant changes in the C−O bond lengths or O−C−O bond angles and a small decrease in the Zn−O bond lengths from ambient pressure to 0.94 GPa.[18] It is worth noting that experimental and theoretical studies revealed significant compressibility of the metal−oxygen polyhedra and rigidity of the organic ligands also for many other MOFs.[40,41] It has also been reported that most MOFs respond to pressure by rotating metal polyhedra.[41] Thus, the mechanism of the pressure-induced phase transition can be rationalized as follows. Application of pressure leads to tilts of the rigid $DCOO^-$ ions, significant shortening of Zn−O distances, and rotation of the ZnO_6 octahedra. This in turn leads to an increase in repulsive forces between the oxygen atoms. To relieve this repulsion, the rigid formate units experience abrupt reorientations near 1.1 GPa, which leads to loss of the 6-fold symmetry axis and significant distortion of the ZnO_6 octahedra. Recent studies of $[tmenH_2][Er(HCOO)_4]$ ($tmenH_2^{2+}$ = *N*,*N*,*N*′,*N*′-tetramethylethylenediammonium) showed that the $tmenH_2^{2+}$ cation does not play a significant role in the phase transformation, but this transformation is associated with major modification in the erbium−oxygen polyhedra.[41] In other words, the pressure-induced bond rearrangement occurs, which is accompanied by a 10% unit cell volume change and significant decrease in the compressibility of the two phases.[41] Our data for $[ND_4][Zn(DCOO)_3]$ also revealed significant distortion of the metal formate framework and smaller compressibility of the high-pressure phase. X-ray diffraction data for the nondeuterated sample show, however, that the phase transformation is not accompanied by any significant decrease of the unit cell volume.[18] The structural modification under pressure is therefore weaker for the studied here $[ND_4][Zn(DCOO)_3]$ compound when compared to $[tmenH_2][Er(HCOO)_4]$. This behavior can be most likely correlated with significantly larger flexibility of the latter compound, as evidenced by the smaller value of the isothermal bulk modulus for $[tmenH_2][Er(HCOO)_4]$ (13.8 GPa) when compared to ammonium zinc formate (32.8 GPa).[18,41]

CONCLUSIONS

We have presented for the first time DFT calculations of vibrational properties for the isolated clusters: the NH_4^+ (ND_4^+) cation in the dimeric complex unit (model 1) and the monomeric $[Zn(HCOO)_6]^{4-}$ ($[Zn(DCOO)_6]^{4-}$) unit (model 2) that allowed precise assignment of modes of the studied compounds. Our temperature-dependent studies show a very weak effect of deuteration on the phase transition temperature and very pronounced broadening of bands related to vibrations of the ammonium cations. Thus, our results prove that the movement of proton (deuteron) along N−H···O (N−D···O) bonds can be excluded as the microscopic origin of the temperature-induced phase transition, and this transition is governed by the rotational dynamics of NH_4^+ (ND_4^+) ions. Since a similar weak isotopic effect was also reported for dimethylammonium analogues, crystallizing in a different $4^{12}\cdot6^3$ topology, it is clear that the topology of the metal formate framework has a weak effect on the phase transition mechanism in this class of MOFs and the major role is played by the protonated amine cations located in the cavities of the framework. It is worth noting that the $[K][Mn(HCOO)_3]$ compound has recently been discovered, which is isomorphous at room temperature to $[NH_4][M(HCOO)_3]$ compounds.[42] However, this potassium compound does present neither ferroelectric phase transition nor disorder. Hence, the substitution of isotropic K^+ ion by a tetrahedral NH_4^+ ion drastically modifies the structural and dynamic behavior. This result is yet another confirmation that H-bonds and ordering of the ammonium ions play an essential role in the mechanism of the phase transition and thus multiferroic behavior of this family of compound at low temperatures. Interestingly, this result indicates a way to modulate the ferroelectric transition temperature and ferroelectric properties by partially replacing the NH_4^+ cations with K^+ cations.

In addition to the temperature-dependent studies, which provided a deeper understanding of the temperature-induced phase transition, we also present pressure dependence of Raman spectra for a representative member of this family of compounds, $[ND_4][Zn(DCOO)_3]$. The major finding of this high pressure study is that $[ND_4][Zn(DCOO)_3]$ exhibits a pressure-induced strongly first-order structural phase transition

dx.doi.org/10.1021/ic501074x | Inorg. Chem. 2014, 53, 9615−9624

near 1.1 GPa, associated mainly with very strong distortion of the metal formate framework. In particular, Raman scattering studies reveal the presence of crystallographically nonequivalent formate ions in the high-pressure phase, with significantly different C−D bond lengths. Thus, in contrast to the temperature-induced phase transition, which has an order−disorder character, the pressure-induced transition is not related to ordering of ammonium cations but a strong distortion of the anionic framework. Although the structural distortion is large, the metal formate framework of the high-pressure phase still has similar connectivity of the structural units as the parent phase and the original hexagonal structure is retained after decompression.

■ ASSOCIATED CONTENT

Supporting Information

Figures S1−S15: Powder X-ray diffraction, DSC traces for $[ND_4][Zn(DCOO)_3]$, imaginary part of the dielectric constant, optimized structure for the NH_4^+ (ND_4^+) cation and $[Zn(HCOO)_6]^{4-}$ ($[Zn(DCOO)_6]^{4-}$), IR and Raman spectra at different temperatures, temperature dependence of bandwidths and wavenumbers, Raman spectra of $[ND_4][Zn(DCOO)_3]$ recorded at different pressures. Tables S1−S3: correlation diagram showing the correspondence between the optical modes in the $P6_322$ and $P6_3$ structures of $[NH_4][Zn(HCOO)_3]$ ($[ND_4][Zn(DCOO)_3]$), calculated and experimental wavenumbers of $[NH_4][Zn(HCOO)_3]$ and $[ND_4][Zn(DCOO)_3]$. This material is available free of charge via the Internet at http://pubs.acs.org.

■ AUTHOR INFORMATION

Corresponding Author

*E-mail: m.maczka@int.pan.wroc.pl. Phone: +48-713954161. Fax: +48-713441029.

Notes

The authors declare no competing financial interest.

■ ACKNOWLEDGMENTS

This research was supported by the National Center for Science (NCN) in Poland under Project No. DEC-2011/03/B/ST5/01019. A generous computer time from the Wrocław Supercomputer and Networking Center is acknowledged. NCN under Project DEC-2011/03/B/ST5/01019.

■ REFERENCES

(1) (a) Wang, K. F.; Liu, J. M.; Ren, Z. F. *Adv. Phys.* **2009**, *58*, 321−448. (b) Hill, N. A. *J. Phys. Chem. B* **2000**, *104*, 6694−6709.

(2) (a) Rogez, G.; Viart, N.; Drillon, M. *Angew. Chem., Int. Ed.* **2010**, *49*, 1921−1923. (b) Ramesh, R. *Nature* **2009**, *461*, 1218−1219.

(3) (a) Wang, Z.; Zhang, B.; Otsuka, T.; Inoue, K.; Kobayashi, H.; Kurmoo, M. *Dalton Trans.* **2004**, 2209−2216. (b) Wang, X. Y.; Gan, L.; Zhang, S. W.; Gao, S. *Inorg. Chem.* **2004**, *43*, 4615−4625.

(4) Wang, Z.; Hu, K.; Gao, S.; Kobayashi, H. *Adv. Mater.* **2010**, *22*, 1526−1533.

(5) Liu, B.; Zhang, R.; Hu, K. L.; Wang, Z. M.; Gao, S. *Inorg. Chem.* **2012**, 13363−13372.

(6) (a) Zhao, J. P.; Hu, B. W.; Lloret, F.; Tao, J.; Yang, Q.; Zhang, X. F.; Bu, X. H. *Inorg. Chem.* **2010**, *49*, 10390−10399. (b) Cañadillas-Delgado, L.; Fabelo, O.; Rodríguez-Velamazán, J. A.; Lemée-Cailleau, M. H.; Mason, S. A.; Pardo, E.; Lloret, F.; Zhao, J. P.; Bu, X. H.; Simonet, V.; Colin, C. V.; Rodríguez-Carvajal, J. *J. Am. Chem. Soc.* **2012**, *134*, 19772−19781.

(7) Hu, K. L.; Kurmoo, M.; Wang, Z.; Gao, S. *Chem.—Eur. J.* **2009**, *15*, 12050−12064.

(8) (a) Liu, J. X.; Shekhah, O.; Stammer, X.; Arslan, H. K.; Liu, B.; Schüpbach, B.; Terfort, A.; Wöll, C. *Mater.* **2012**, *5*, 1581−1592. (b) Kuppler, R. J.; Timmons, D. J.; Fang, Q. R.; Li, J. R.; Makal, T. A.; Young, M. D.; Yuan, D.; Zhao, D.; Zhuang, W.; Zhou, H. C. *Coord. Chem. Rev.* **2009**, *253*, 3042−3066.

(9) (a) Jain, P.; Dalal, N. S.; Toby, B. H.; Kroto, H. W.; Cheetham, A. K. *J. Am. Chem. Soc.* **2008**, *130*, 10450−10451. (b) Jain, P.; Ramachandran, V.; Clark, R. J.; Zhou, H. D.; Toby, B. H.; Dalal, N. S.; Kroto, H. W.; Cheetham, A. K. *J. Am. Chem. Soc.* **2009**, *131*, 13625−1327. (c) Fu, D. W.; Zhang, W.; Cai, H. L.; Zhang, Y.; Ge, J. Z.; Xiong, R. G.; Huang, S. D.; Nakamura, T. *Angew. Chem., Int. Ed.* **2011**, *50*, 11947−11951. (d) Wang, W.; Yan, L. Q.; Cong, J. Z.; Zhao, Y. L.; Wang, F.; Zhen, S. P.; Zou, T.; Zhang, D.; Wang, S. G.; Han, X. F.; Sun, Y. *Sci. Rep.* **2013**, *3*, 2024.

(10) Guo, M.; Cai, H. L.; Xiong, R. G. *Inorg. Chem. Commun.* **2010**, *13*, 1590−1598.

(11) Sanchez-Andujar; Presedo, S.; Yanez-Vilar, S.; Castro-Garcia, S.; Shamir, J.; Senaris-Rodriguez, M. A. *Inorg. Chem.* **2010**, *49*, 1510−1516.

(12) Pato-Doldan, B.; Sanchez-Andujar, M.; Gomez-Aguirre, L. C.; Yanez-Vilar, S.; Lopez-Beceiro, J.; Gracia-Fernandez, C.; Haghighirad, A. A.; Ritter, F.; Castro-Garcia, S.; Senaris-Rodriguez, M. A. *Phys. Chem. Chem. Phys.* **2012**, *14*, 8498−8501.

(13) Stroppa, A.; Jain, P.; Barone, P.; Marsman, M.; Perez Mato, J. M.; Cheetham, A. K.; Kroto, H. W.; Picozzi, S. *Angew. Chem., Int. Ed.* **2011**, *50*, 5847−5850.

(14) Stroppa, A. *J. Phys. Conf. Ser.* **2013**, *428*, 012029.

(15) (a) Stroppa, A.; Barone, P.; Jain, P.; Perez-Mato, J. M.; Picozzi, S. *Adv. Mater.* **2013**, *25*, 2284−2290. (b) Di Sante, D.; Stroppa, A.; Jain, P.; Picozzi, S. *J. Am. Chem. Soc.* **2013**, *135*, 18126−18130.

(16) (a) Wang, Z.; Zhang, B.; Inoue, K.; Fujiwara, H.; Otsuka, T.; Kobayashi, H.; Kurmoo, M. *Inorg. Chem.* **2007**, *46*, 437−445. (b) Xu, G. C.; Zhang, W.; Ma, X. M.; Hen, Y. H.; Zhang, L.; Cai, H. L.; Wang, Z. M.; Xiong, R. G.; Gao, S. *J. Am. Chem. Soc.* **2011**, *133*, 14948−14951.

(17) (a) Mączka, M.; Pietraszko, A.; Macalik, B.; Hermanowicz, K. *Inorg. Chem.* **2014**, *53*, 787−794. (b) Zhang, R.; Xu, G. C.; Wang, Z. M.; Gao, S. *Chem.—Eur. J.* **2013**, *20*, 1146−1158.

(18) Li, W.; Probert, M. R.; Kosa, M.; Bennett, T. D.; Thirumurugan, A.; Burwood, R. P.; Parinello, M.; Howard, J. A. K.; Cheetham, A. K. *J. Am. Chem. Soc.* **2012**, *134*, 11940−11943.

(19) (a) Mączka, M.; Gągor, A.; Macalik, B.; Pikul, A.; Ptak, M.; Hanuza, J. *Inorg. Chem.* **2014**, *53*, 457−467. (b) Mączka, M.; Ptak, M.; Macalik, L. *Vibr. Spectrosc.* **2014**, *71*, 98−104.

(20) (a) Nibbering, E. T. J.; Dreyer, J.; Kühn, O.; Bredenbeck, J.; Hamm, P.; Elsaesser, T. *Chem. Phys.* **2007**, *87*, 619−687. (b) Sobczyk, L.; Obrzyd, M.; Filarowski, A. *Molecules* **2013**, *18*, 4467−4476.

(21) Carabatos-Nedelec, C.; Becker, P. *J. Raman Spectrosc.* **1997**, *28*, 663−671.

(22) Cummins, H. Z.; Levanyuk, A. P. *Light Scattering Near hase Transitions*; North-Holland Publishing Company: 1983; pp 7−122.

(23) (a) Becke, A. D. *J. Chem. Phys.* **1996**, *104*, 1040−1046. (b) Becke, A. D. *J. Chem. Phys.* **1993**, *98*, 5648−5652. (c) Lee, C.; Yang, W.; Parr, R. G. *Phys. Rev. B* **1988**, *37*, 785−789. (d) Ditchfield, R.; Hehre, W. J.; Pople, J. A. *J. Chem. Phys.* **1971**, *54*, 724−728.

(24) (a) Joselin Beaula, T.; Manimaran, D.; Hubert Joe, I.; Rastogi, V. K.; Bena Jothy, V. *Spectrochim. Acta, Part A* **2014**, *126*, 170−177. (b) Gnanasambandan, T.; Gunasekaran, S.; Seshadri, S. *Spectrochim. Acta, Part A* **2013**, *112*, 52−61.

(25) Magalhaes, A. L.; Madail, S. R. R. S.; Ramos, M. *J. Theor. Chem. Acc.* **2000**, *105*, 68−76.

(26) Suresh, D. M.; Amalanathan, M.; Sebastian, S.; Sajan, D.; Hubert Joe, I.; Bena Jothy, V.; Nemec, I. *Spectrochim. Acta, Part A* **2013**, *115*, 595−602.

(27) Dunning, T. H., Jr.; Hay, P. J. In *Modern Theoretical Chemistry*; Schaefer, H. F., Ed.; Plenum: New York, 1976; Vol. 3, pp 1−28.

(28) Michalska, R.; Wysokiński, R. *Chem. Phys. Lett.* **2005**, *403*, 211−217.

(29) Frisch, M. J.; Trucks, G. W.; Schlegel, H. B.; Scuseria, G. E.; Robb, M. A.; Cheeseman, J. R.; Scalmani, G.; Barone, V.; Mennucci, B.; Petersson, G. A.; Nakatsuji, H.; Caricato, M.; Li, X.; Hratchian, H. P.; Izmaylov, A. F.; Bloino, J.; Zheng, G.; Sonnenberg, J. L.; Hada, M.; Ehara, M.; Toyota, K.; Fukuda, R.; Hasegawa, J.; Ishida, M.; Nakajima, T.; Honda, Y.; Kitao, O.; Nakai, H.; Vreven, T.; Montgomery, J. A., Jr.; Peralata, J. E.; Ogliaro, F.; Bearpark, M.; Heyd, J. J.; Brothers, E.; Kudin, K. N.; Staroverov, V. N.; Kobayashi, R.; Normand, J.; Raghavachari, K.; Rendell, A.; Burant, J. C.; Iyengar, S. S.; Tomasi, J.; Cossi, M.; Rega, N.; Millam, J. M.; Klene, M.; Knox, J. E.; Cross, J. B.; Bakken, V.; Adamo, C.; Jaramillo, J.; Gomperts, R.; Stratmann, R. E.; Yazyev, O.; Austin, A. J.; Cammi, R.; Pomelli, C.; Ochterski, J. W.; Martin, R. L.; Morokuma, K.; Zakrzewski, V. G.; Voth, G. A.; Salvador, P.; Dannenberg, J. J.; Dapprich, S.; Daniels, A. D.; Farkas, O.; Foresman, J. B.; Ortiz, J. V.; Cioslowski, J.; Fox, D. J. *Gaussian 09*; Gaussian, Inc.; Wallingford, CT, 2009.
(30) (a) Barone, V.; Biczysko, M.; Pavone, M. *Chem. Phys.* **2008**, *346*, 247−256. (b) Grimme, S. *Wiley Interdisciplinary Reviews: Computational Molecular Science* **2011**, *1*, 211−228.
(31) (a) Albuquerque, A. R.; Garzim, M. L.; Dos Santos, I. M. G.; Longo, V.; Longo, E.; Sambrano, J. R. *J. Phys. Chem. A* **2012**, *116*, 11731−11735. (b) Hunter, S. High-pressure computational and experimental studies of energetic materials. Doctoral Thesis, University of Edinburgh, 2013.
(32) (a) Samet, A.; Ben Ahmed, A.; Mlayah, A.; Boughzala, H.; Hlil, E. K.; Abid, Y. *J. Mol. Struct.* **2010**, *977*, 72−77. (b) Wojtaś, M.; Bator, G.; Baran, J. *Vibr. Spectrosc.* **2003**, *33*, 143−152.
(33) (a) Hadrich, A.; Lautie, A.; Mhiri, T. *J. Raman Spectrosc.* **2000**, *31*, 587−593. (b) Kruger, A.; Heyns, A. M. *Vib. Spectrosc.* **1997**, *14*, 171−181. (c) Fredrickson, R. L.; Decius, J. C. *J. Chem. Phys.* **1977**, *66*, 2297−2305.
(34) Maczka, M.; Hanuza, J.; Kaminskii, A. A. *J. Raman Spectrosc.* **2006**, *37*, 1257−1264.
(35) (a) Wang, C. H.; Wright, R. B. *J. Chem. Phys.* **1973**, *58*, 1411−1419. (b) Balusubramanian, M.; Ramakrishnan, V.; Rajendran, S. *Pramana - J. Phys.* **1991**, *36*, 603−610. (c) Samantaray, R.; Clark, R. J.; Choi, E. S.; Dalal, N. S. *J. Am. Chem. Soc.* **2012**, *134*, 15953−15962.
(36) (a) Berger. *J. Phys. C* **1975**, *8*, 2903−2910. (b) Ayala, A. P.; Henriques Neto, J. M.; Paschoal, C. W. A.; Guedes, I.; Sasaki, J. M.; Freire, P. T. C.; Melo, F. E. A.; Medes Filho, J.; Leyva, A. G.; Polla, G.; Vega, D.; Perazzo, P. K. *J. Raman Spectrosc.* **2000**, *31*, 491−495. (c) Heyns, A. M. *J. Chem. Phys.* **1986**, *84*, 3610−3616.
(37) Asaji, T.; Ishizaka, T. *Z. Naturforsch.* **2000**, *55*, 83−89.
(38) Maczka, M.; Souza Filho, A. G.; Paraguassu, W.; Freire, P. T. C.; Mendes Filho, J.; Hanuza, J. *Prog. Mater. Sci.* **2012**, *57*, 1335−1381.
(39) Durben, D. J.; McMillan, P. F.; Wolf, G. H. *Am. Mineral.* **1993**, *78*, 1143−1148.
(40) (a) Kosa, M.; Tan, J. C.; Merrill, C. A.; Krack, M.; Cheetham, A. K.; Parinello, M. *ChemPhysChem* **2010**, *11*, 2332−2336. (b) Tan, J. C.; Cheetham, A. K. *Chem. Soc. Rev.* **2011**, *40*, 1059−1080.
(41) Spencer, E. C.; Kiran, M. S. R. N.; Li, W.; Ramamurty, U.; Ross, N. L.; Cheetham, A. K. *Angew. Chem., Int. Ed.* **2014**, *53*, 5583−5586.
(42) Duan, Z.; Wang, Z.; Gao, S. *Dalton Trans.* **2011**, *40*, 4465−4473.